Thermodynamics of a quark-gluon plasma at finite baryon density

Z. V. Khaidukov[1,2] and Yu. A. Simonov[2]

[1]*Moscow Institute of Physics and Technology, Institutskiy pereulok 9, 141700 Dolgoprudny, Moscow Region, Russia*

[2]*Institute for Theoretical and Experimental Physics, NRC "Kurchatov Institute," B. Cheremushkinskaya 25, Moscow 117259, Russia*

(Received 27 June 2019; revised manuscript received 18 September 2019; published 14 October 2019)

Properties of the quark-gluon plasma (QGP) in the presence of the baryon chemical potential μ_B are studied using the field correlator method (FCM). The nonperturbative FCM dynamics includes the Polyakov line, computed via color-electric string tension $\sigma^E(T)$, and the quark and gluon Debye masses, defined by the color-magnetic string tension $\sigma^H(T)$. The resulting QGP thermodynamics at $\mu_B \leq 400$ MeV is in a good agreement with the available lattice data; neither the pressure nor the sound velocity shows any sign of a critical behavior in this region.

DOI: 10.1103/PhysRevD.100.076009

I. INTRODUCTION

The main result of heavy ion experiments, performed over the last 15 years at the Relativistic Heavy Ion Collider (RHIC) and then at the LHC, is the discovery of a new form of matter [1–5] with its properties markedly different from the pre–RHIC era predictions; see Refs. [6–15] and references therein. Instead of the commonly assumed picture of a weakly interacting quark-gluon plasma (QGP), one possibly has a strongly coupled liquid subject to the law of the relativistic hydrodynamics [16–18]. The properties of the produced matter drastically change during several stages of evolution: from the stage of formation, hydrodynamization, and thermalization toward the hadron gas production. The wealth of the QCD matter phases is reflected in the QCD phase diagram drawn in the (μ, T) plane. However, the correspondence between the specific (μ, T) domains of the phase diagram and the space-time dynamics of the fireball should be considered with caution. The reason is that the phase diagram describes the limit of an infinite system in thermodynamic equilibrium.

From the theoretical viewpoint, the matter created in heavy ion collisions should be described by the fundamental laws of QCD. For these reasons, the dynamics and thermodynamics of QCD at finite temperatures is now the focus of numerous investigations. At this moment, one of the main sources of information is the lattice calculations. The presence of strong interaction in QGP at zero baryon density has been demonstrated in numerous studies [19–24]. They show that the ratio of the QGP pressure to the noninteracting case is less than 0.8 and remains almost constant with increasing temperature.

Another striking discovery in this domain is the analysis of the temperature transition, made in the $2+1$ QCD lattice computations, which has shown a smooth crossover in the temperature region $T = 140 \div 180$ MeV [25].[1]

Despite dramatic progress, the question about the structure of the QCD phase diagram at nonzero baryon density remains open. This happens mostly because lattice methods are strongly restricted to a domain of small chemical potentials[2] ($N_c = 3$) due to the "sign problem." To circumvent this difficulty in the case of $N_c = 3$, one can use the Taylor expansion around zero chemical potential [31,32] or use imaginary chemical potential[33]. Another possibility is to decrease the number of colors to $N_c = 2$, where the sign problem is absent [34–37].

From all these facts, the need for analytic methods that can help with investigation of QGP thermodynamics and QCD phase diagram becomes obvious. In this paper, we will focus on the field correlator method (FCM), which is applicable in QCD at any chemical potential and any

[1]This QCD crossover is a new phenomenon, possibly having some analogues in the material sciences and in the ionization and dissociation processes. The question of the existence of a critical point at finite baryon chemical potential is still of intense interest [26].

[2]We want to point out that another very important source of information of QCD phase diagram is connected with neutron stars physics [27]. LIGO and Virgo's discovery of gravitational waves from a neutron star [28] opened a new era of quark matter studies. Possible discovery of quark stars will give much more opportunities for studying the QCD phase diagram [29,30].

temperature [38–43]. In this method, the nonperturbative dynamics in confinement and deconfinement regions is based on vacuum properties, described by gluonic field correlators [38–52], and the key role is played by correlators of color-electric fields D^E and color-magnetic fields D^H, which provide color-electric confinement with the string tension $\sigma^E(T)$ and color-magnetic confinement (CMC) with the string tension $\sigma^H(T)$. The latter, being calculated from field correlators and on the lattice, grows with T, $\sigma^H(T) \sim g^4(T)T^2$ and ensures the strong interaction at large T mentioned above. It is interesting to note that in the FCM the crossover phenomenon is connected with the gradual vanishing of the vacuum confining correlator $D^E(z)$ [and the resulting string tension $\sigma^E(T)$] with the growing temperature. The same phenomenon of the "melting confinement" can be observed in the SU(3) gluodynamics [49], in which the string tension $\sigma(T)$, measured on the lattice [53–56] is also decreasing with T, but in the case of SU(3), it cannot smoothly match the fast-growing gluon pressure (in contrast to the slowly growing glueball pressure due to large glueball masses greater than or approximately equal to 2 GeV). As a result, one has a weak first-order transition in SU(3) [49], while in the $n_f = 2 + 1$ QCD with low mass mesons, the smooth matching of pressure is achievable in the course of transition.

For proof of this picture, one can use the quark condensate vanishing with T [19,23,57] in the same way, as $\sigma(T)$ (see, e.g., Fig. 4 in Ref. [53] and Fig. 6 in Ref. [55] with Fig. 4 in Ref. [19]), which is connected with confinement via $\langle\bar{q}q\rangle \sim \sigma^{3/2}$ [58–60], and almost the same reasoning can extend this connection to nonzero T.

One can see many important questions in QCD that could be investigated by the FCM, and we will focus on one of them; the main task of this paper is to give a self-consistent description of QGP at nonzero μ_B.

We shall use below the thermodynamic formalism exploited before for the gluon plasma in [48–50], and extended to the QGP case in Refs. [51,52].

The paper is organized as follows. In Sec. II, we introduce the FCM in the case of finite temperature and chemical potential. In Sec. III, we calculate the Polyakov line in the case of $(2 + 1)n_f$ QCD. In Sec. IV, we extend the FCM formalism to nonzero μ_B. In Sec. V, we compare our results with lattice data at zero and finite baryon chemical potential. Section VI is devoted to conclusions and the outlook.

II. FIELD CORRELATOR METHOD AT FINITE TEMPERATURE

The FCM is a very powerful tool for describing physics of QCD (see Ref. [61] for a recent review), which allows us to formulate "confinement" or in other words to obtain the area law of the Wilson loop in terms of the vacuum background fields, with the field correlators D^E and D^H ensuring color-electric and color-magnetic confinement with the string tensions σ^E and σ^H. As a result, all hadron masses are defined in this method only by fermion masses and string tension σ^E.

All gluon fields A_μ in QCD in the framework of the background perturbation theory [62] can be divided into vacuum background part B_μ and perturbative part a_μ, $A_\mu = B_\mu + a_\mu$, with B_μ contributing to σ^E and σ^H, while a_μ is treated in the background perturbation theory with the perturbative coupling constant $\alpha_s(Q)$, defined by the scale parameter $\Lambda_{\rm QCD}$.

For the hadron spectrum in QCD and for the QCD thermodynamics, the basic role is played by the background fields B_μ, while a_μ yield perturbative corrections. On the other hand, in high momentum processes with $Q^2 \gg M_B^2 = 2\pi\sigma = O(1\ \text{GeV})$, the basic role is played by the perturbative fields a_μ. The boundary M_B^2 found in Ref. [63] separates both types of dynamics, and σ itself defines the scale $\Lambda_{\rm QCD}$ [61]. In this sense, the fields B_μ and a_μ can be associated with the regions $Q^2 \le M_B^2$ and $Q^2 > M_B^2$, respectively.

In thermodynamics at temperatures $T \le M_B$, the basic dynamics is given by the background fields B_μ, which define both color-magnetic confinement (yielding CMC Debye screening) and Polyakov line interactions. In what follows, we shall concentrate on these contributions, taking into account gluon exchange corrections. The fundamental role in FCM is played by the quadratic gluonic field correlator. It consists of two terms, D and D_1,

$$\begin{aligned} D_{\mu\nu\lambda\rho} &= g^2 \mathrm{tr}_a < F_{\mu\nu}(x)\Phi(x,y)F_{\lambda\rho}(y)\Phi(y,x) \\ &>= (\delta_{\mu\lambda}\delta_{\nu\rho} - \delta_{\mu\rho}\delta_{\nu\lambda})D(x-y) \\ &\quad + \frac{1}{2}\left[\frac{\partial}{\partial_\mu}(x_\lambda\delta_{\nu\rho} - x_\rho\delta_{\nu\lambda}) + (\mu\lambda \leftrightarrow \nu\rho)\right]D_1(x-y). \end{aligned} \tag{1}$$

Here, the parallel transporter $\Phi(x,y) = P\exp(ig\int_y^x du_\nu A_\nu(u))$, and the fields F_{i4} and F_{4i} refer to D^E and D_1^E correlators, and F_{ik} refers to the D^H and D_1^H correlators. One can obtain string tension via D^E and D^H:

$$\sigma^{E,H} = \frac{1}{2}\int D^{E,H} d^2 z. \tag{2}$$

At zero temperature, $\sigma^E = \sigma^H$. Let us discuss in more detail the basic principles of the FCM at finite temperatures. We must take into account that at finite temperatures the confinement-deconfinement transition occurs. In our formalism, that means that the electric string (or color-electric correlator D^E) has to vanish. But there are no restrictions on the value of color-magnetic correlator (or alternatively on the existence of color-magnetic string tension σ_H).

As shown by analytic [64] and lattice studies, σ_H grows quadratically with temperature. As a result, for $T > T_c$, there is no confining string between color charges, but there is still nonperturbative interaction between them, i.e., color-electric (CE) interaction, contained in the Polyakov line $L(T)$, and the color-magnetic (CM) confinement in a spatial projection of the Wilson loop. Analysis of physics of QGP in terms of the FCM made in Refs. [44–47,65,66] also confirmed the important role of Polyakov loops for the description of thermodynamic of GP and QGP. In Refs. [48–52], also, the CMC interaction was taken into account, providing a self-consistent dynamical picture in a good agreement with lattice data. As for CMC, it is the main interaction in QGP, operating above the transition temperature, as was observed in lattice data [67], in which the CMC correlators $\langle \mathrm{tr} F_{ik}(x)\Phi(x,y)F_{ik}(y)\rangle$ have been measured; see also Ref. [68], in which σ^H was studied on the lattice, and Ref. [64], in which σ^H was estimated in the FCM.

It was found in Ref. [69] that CMC does not support white bound states in $q\bar{q}$ and gg systems at zero temperature; however, it can create the screening mass $M(T)$ of isolated quarks and gluons [48–51,64], which grows with temperature so that the ratio $\frac{M(T)}{T}$ is constant up to the logarithmic terms.

As was shown in Refs. [44–52], the most convenient for description of QCD thermodynamics is the T-dependent path integral (worldline) formalism, in which the pressure can be written in the form[44,47,49] (see Appendix A for details of the derivation)

$$P_{gl} = 2(N_c^2 - 1)\int_0^\infty \frac{ds}{s}\sum_{n=1,2\ldots} G^n(s). \tag{3}$$

Here, s is the proper time, and for $G^n(s)$, one can obtain

$$G^n(s) = \int (Dz)^\omega_{\mathrm{on}} \exp(-K)\hat{\mathrm{tr}}_a \langle W^a_\Sigma(C_n)\rangle, \tag{4}$$

where $K = \frac{1}{4}\int_0^s d\tau (\frac{dz^\mu}{d\tau})^2$ and $W^a_\Sigma(C_n)$ is the adjoint Wilson loop defined for the gluon path C_n, which has both temporal (i4) and spacial (ij) projections and $\hat{\mathrm{tr}}_a$ is the normalized adjoint trace. When $T > T_c$, the correlation function between CE and CM fields is rather weak [44]:

$$\langle E_i(x)B_k(y)\Phi(x,y)\rangle \approx 0. \tag{5}$$

At this point, when averaging $W^a_\Sigma(C_n)$ in (4), one should take into account that the paths of gluons at $n_0 \neq 0$ are not closed, and there is a free piece of n temporal steps, which should be connected by the gluon path to form a closed contour of the Wilson loop, with the area law in the vacuum confining field. Therefore, one can add before vacuum averaging a piece along the time axis, which closes the gluon trajectory from n_0 to $n = 0$ and back from $n_q = 0$ to $n = n_0$ (which is an identical operation yielding a factor 1). In this way, one obtains a product of a closed contour and a Polyakov line from 0 to n_0, and the vacuum averaging yields the expression for the factorized Wilson loops [49],

$$\langle W^a_\Sigma(C_n)\rangle = L^{(n)}_{\mathrm{adj}}(T)\langle W_3\rangle, \tag{6}$$

with $L^{(n)}_{\mathrm{adj}} \approx L^n_{\mathrm{adj}}$ for $T \leq 1$ GeV. One can integrate out the z_4 part of the path integral $(Dz)^\omega_{\mathrm{on}} = (Dz_4)^\omega_{\mathrm{on}} D^3 z$, with the result

$$G^{(n)}(s) = G^{(n)}_4(s)G_3(s),$$
$$G^n_4(s) = \int (Dz_4)^\omega_{\mathrm{on}} e^{-K} L^{(n)}_{\mathrm{adj}} = \frac{1}{2\sqrt{4\pi s}} e^{-\frac{n^2}{4T^2 s}} L^{(n)}_{\mathrm{adj}}. \tag{7}$$

This factorization holds also for quarks and will be used below (with the change of the adjoint representation to the fundamental one).

The resulting gluon contribution is

$$P_{gl} = \frac{2(N_c^2-1)}{\sqrt{4\pi}}\int_0^\infty \frac{ds}{s^{3/2}} G_3(s) \sum_{n=1,2,\ldots} e^{-\frac{n^2}{4T^2 s}} L^n_{\mathrm{adj}},$$
$$G_3(s) = \int (D^3 z)_{xx} e^{-K_{3d}} \langle \hat{\mathrm{tr}}_a W^a_3\rangle. \tag{8}$$

The direct appearance of $L^{(n)}_{\mathrm{adj}}(T)$ in the thermodynamic potential is an important feature of the present nonperturbative formalism based on the FCM. It was derived before in Ref. [44], in which the CMC was not taken into account, and the origin of $L^{(n)}$ was associated only with the correlator D_1^E [65]. As will be shown below, the mechanism of the Polyakov loop is much more complicated, and we shall compute $L(T)$ in a different way.

At this point, we are coming to the problem of the CMC and its contribution to the gluon dynamics.

As is well known [66], the CMC generates the nonperturbative Debye mass $M_D(T)$, connected to the CM string tension $\sigma^H(T)$, which is proportional to T^2,

$$\sigma^H(T) = \mathrm{const}\, g^4(T)T^2,$$

as it was found on the lattice [68] and nonperturbatively in the Appendix of Ref. [64]. The exact calculation of $G_3(s)$, which should give the explicit dependence on $M_D(T)$, is, however, difficult, and therefore one can use approximations explained in Appendix B.

The inclusion of color-magnetic interaction leads to the generation of a nonperturbative Debye mass M_D for gluons and quarks. For gluons $M_{\mathrm{adj}} \sim \sqrt{\sigma^H(T)}$, one can take it into account by an approximate expression for the third Green's function [49], which is derived in Appendix B,

$$G_3(s) = \frac{1}{(4\pi s)^{3/2}} \sqrt{\frac{(M^2_{\rm adj})s}{\sin h(M^2_{\rm adj})s}}. \quad (9)$$

It should be mentioned that the resulting gluon pressure (8) is in good agreement with the lattice data [49].

In the noninteracting case, i.e., $\sigma^H = 0$ and $L_{\rm adj} = 1$, one obtains the ideal gas pressure:

$$P_{gl} = P_0 = \frac{(N_c^2 - 1)}{45}\pi^2 T^4. \quad (10)$$

For quarks, one can write the expression in the same form as in (8), but with the quark mass term $e^{-m_q^2 s}$:

$$P_f = \sum_{q=u,d,s} P_q,$$
$$P_q = \frac{4N_c}{\sqrt{4\pi}} \int_0^\infty \frac{ds}{s^{3/2}} e^{-m_q^2 s} S_3(s) \sum_{n=1,2,\ldots} (-)^{n+1} e^{-\frac{n^2}{4T^2 s}} L_f^n \quad (11)$$

$$S_3(s) = \frac{1}{(4\pi s)^{3/2}} \sqrt{\frac{(M_f^2)s}{\sin h(M_f^2)s}},$$
$$M^2_{\rm adj} = \frac{9}{4} M_f^2, \qquad L_f^n = (L^n_{\rm adj})^{4/9}. \quad (12)$$

And again in the case of massless noninteracting fermions, one obtains

$$P_f = N_c N_f \frac{7T^4}{180}. \quad (13)$$

The full pressure reads as

$$P_{\rm tot} = P_f + P_{gl}. \quad (14)$$

Integrating over proper time interval ds in (11) and replacing the square root term in (12) by an approximate exponential term [50,52], one obtains

$$P_f = \sum_{q=u,d,s} P_q,$$
$$\frac{P_q(T,\mu)}{T^4} = \frac{2N_c}{\pi^2} \sum_n \frac{(-)^{n+1}}{n^2} L^n K_2\left(\frac{\bar{M}n}{T}\right)\frac{\bar{M}^2}{T^2}, \quad (15)$$

where $\overline{M} = \sqrt{m_f^2 + \frac{M^2(T)}{4}}$, $M(T) = a\sqrt{\sigma_s(T)}$, $a \approx 2$ [51,66].

To include the effects of the baryon chemical potential, we should do the substitution in (11):

$$L_f^n \to L_f^n \cos h(\mu n/T). \quad (16)$$

III. POLYAKOV LINE CALCULATIONS

As we saw, the thermodynamics of QGP in the FCM is defined by two main ingredients: the non-perturbative screening masses $M(T)$ are calculated via $\sigma^H(T)$ and known both analytically and on the lattice [66,68]. This part is especially important at high T due to the growth of $\sigma^H(T)$. Another important ingredient is the Polyakov line L with the dynamics defined by the field correlators D^E and D_1^E [65]. The Polyakov line was introduced in Refs. [44–47] as a main dynamical ingredient of qgp, and it is associated with the correlator $D_1(x)$, which produces the interaction term $V_1(r,T)$, with a nonzero asymptotics $V_1^E(\infty,T)$ so that the Polyakov line is written as $L(T) = \exp(-\frac{V_1(\infty,T)}{2T})$.

However, more careful analysis done in Ref. [70] has revealed that there are three sources of the Polyakov line in the nonperturbative correlators (1): two of them are due to

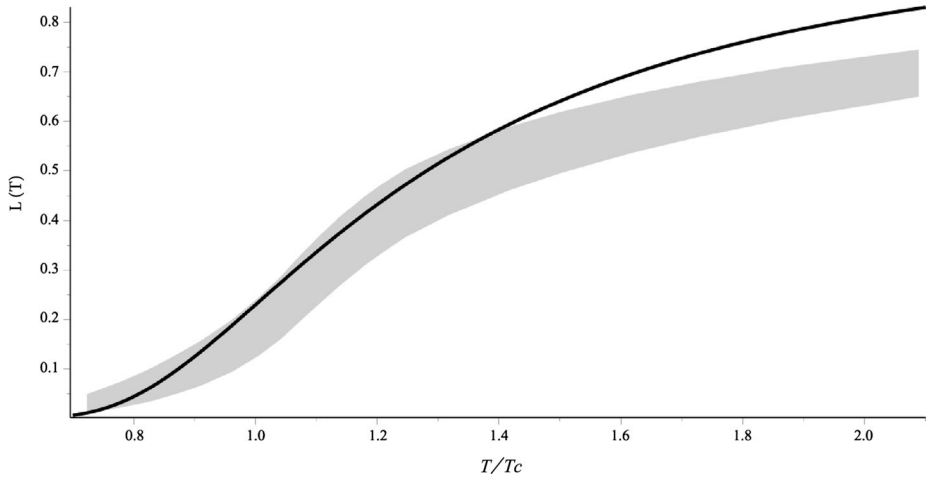

FIG. 1. The Polyakov line as a function of T/T_c,$T_c = 160$ MeV. The gray band corresponds to $L_{\rm HL}$ within the accuracy limits of $a(T)$. The solid black line is the ideal $L_{\rm FCM}$ used below in the paper.

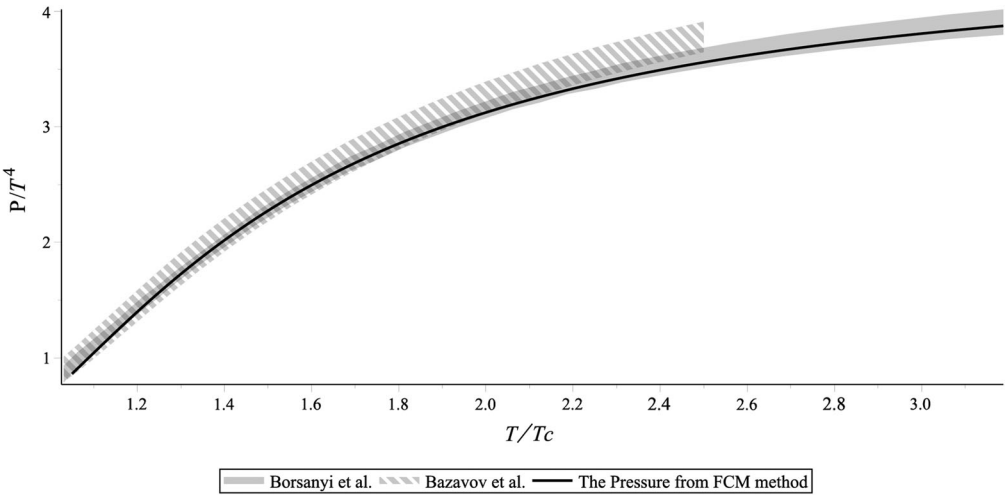

FIG. 2. The ratio of the pressure to T^4 as a function of T/T_c. The gray band is the lattice data of Borsanyi *et al.* [20], and the striped band is the lattice data from Bazavov *et al.* [23].

the correlator $D^E(x)$, and one is due to $D_1^E(x)$, which also generates the perturbative part of $L(T)$. We relegate the detailed analysis of these sources to Appendix C and Ref. [70], and here we only conclude that the main part of the contribution of $D_1^E(x)$ $[V_1^E(\infty, T)]$ is canceled by that of the saturated part of $D^E(x)$ and the resulting contribution can be associated with the confining interaction of the static charge of the Polyakov line with a picked-up antiquark, which create the heavy-light system with mass $M_{\rm HL}(T)$, so that one can continue the previous definition of $L(T)$ as

$$L(T) = \exp\left(-\frac{V_1(\infty, T)}{2T}\right) \to \exp\left(-\frac{M_{\rm HL}(T)}{T}\right).$$

One of the ways to calculate L is to evaluate it via the heavy-light mass $M_{\rm HL}$ [71]. Here, we are using, as in Ref. [71], the mass $M_{\rm HL}(T)$, which is T dependent due to the temperature-dependent string tension $\sigma^E(T)$, studied repeatedly on the lattice [53–55], with the relation $M_{\rm HL}(T) \sim \sqrt{\sigma^E(T)}$. To find $\sigma^E(T)$ explicitly, one can use a connection between σ^E and the quark condensate $\langle\bar{q}q\rangle$ found in Refs. [60,61], which can be associated with the T-dependent quark condensate, since in the FCM approach the latter is produced by the scalar confinement [58–61]. Indeed, the lattice data on $\sigma(T)$ [53–55] and $\bar{q}q(T)$ [19,23,57] show similar behavior.

We take the CE string tension in the massless quark limit related to the chiral condensate [60] as $|\langle\bar{q}q(T)\rangle| = \text{const}\,(\sigma(T))^{3/2}$. Introducing a dimensionless parameter $a(T)$ as $\sigma(T) = \sigma(0)a^2(T)$, one has

$$|\langle\bar{q}q\rangle(T)| = |\langle\bar{q}q\rangle(0)|a^3(T). \tag{17}$$

As a result, one has $M_{\rm HL}(T) = M_{\rm HL}(T_0)\frac{a(T)}{a(T_0)}$ and $L(T) = \exp\left(-\frac{M_{\rm HL}(T)}{T}\right)$. The numerical data are shown in Fig. 1. The error band in Fig. 1 corresponds to the accuracy of $a(T)$ in the lattice data in Ref. [23], and the solid black line is our "ideal" FCM line $L_{\rm FCM}(T)L_{\rm FCM}$, which on one hand is close to the error band and on the other hand, as will be seen below in the paper, yields good agreement with lattice data.

IV. QCD THERMODYNAMICS AT FINITE BARYON CHEMICAL POTENTIAL

One of immediate tests of the FCM thermodynamics is the behavior of the QGP pressure (Fig. 2), the scale

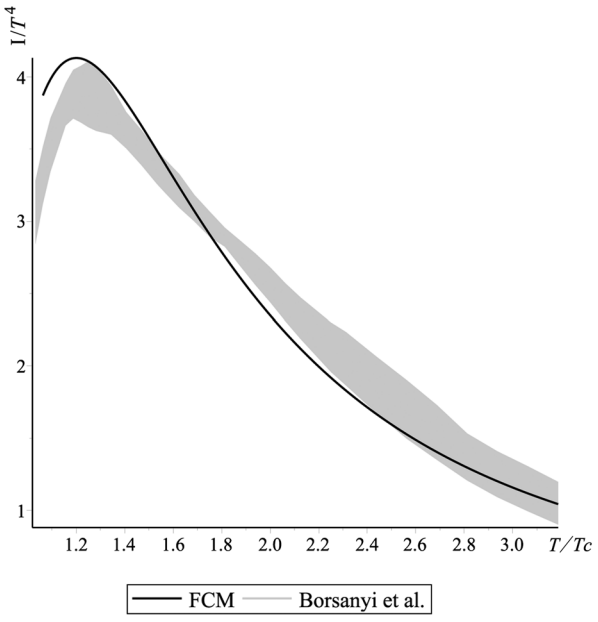

FIG. 3. The ratio of the anomaly $(I = \epsilon - 3P)$ to T^4 in QGP as a function of T/T_c. The gray band is the lattice data of Borsanyi *et al.* [20].

anomaly (Fig. 3), and the speed of sound (Fig. 4), in which $L_{\rm FCM}(T)$ and the CMC Debye mass are taken into account, in comparison with lattice data for zero and the extension to nonzero baryon chemical potential. One can see that our predictions are in good agreement with lattice data at $\mu = 0$.[3]

At this point, we extend our results to a finite baryon chemical potential. We will use the definition of the baryon chemical potential the same way as in Ref. [51], i.e., $\mu_B = 3\mu_q$ (we will not include a separate chemical potential for the strange quark). There is the possibility of comparison of our predictions with the Taylor expansion of μ [32]. We use the following assumption: according to Refs. [46,73], at small densities, $\mu_B \leq 300$–400 MeV, we can neglect the influence of the baryon chemical potential on the Polyakov line.

The summation over n in (15) can be done if one uses the integral representation

$$K_\nu(z) = \frac{(\frac{z}{2})^\nu \Gamma(\frac{1}{2})}{\Gamma(\nu+\frac{1}{2})} \int_0^\infty e^{-z\cosh t} (\sinh t)^{2\nu} dt. \tag{18}$$

As a result, one obtains as in Ref. [51]

$$\frac{1}{T^4} P_q(T,\mu) = \frac{N_c}{\pi^2} (\xi_1^{(+)} + \xi_1^{(-)}) \tag{19}$$

with

$$\xi_1^{(\pm)} = \frac{1}{3}\left(\frac{\bar{M}}{T}\right)^4 \int_0^\infty \frac{u^4 du}{\sqrt{1+u^2}\left[1+\exp\left(\frac{\bar{M}}{T}\sqrt{1+u^2}+\frac{V_1}{2T}\pm\frac{\mu}{T}\right)\right]}. \tag{20}$$

Changing the integration variable,

$$\frac{\bar{M}}{T}\sqrt{1+u^2} = z + \frac{\bar{M}}{T}. \tag{21}$$

The expression (15) can be brought to the form

$$\frac{P_q(T,\mu)}{T^4} = f_+(T,\mu) + f_-(T,\mu), \tag{22}$$

$$f_\pm(T,\mu) = \frac{N_c}{3\pi^2} \int_0^\infty \frac{dz(z^2+2z\frac{\bar{M}}{T})^{3/2}}{1+\exp\left(z+\frac{\bar{M}}{T}+\frac{V_1(T)}{2T}\mp\frac{\mu}{T}\right)}, \tag{23}$$

where it is taken into account that $L = \exp(-V_1(T)/2T)$.

The expression (22) has no singularities at real μ, but $f^\pm$ may get a singularity for imaginary chemical potentials for $\mathrm{Im}(\mu) = \pi T$ due to the vanishing of the denominator in (23) at $z = -\frac{\bar{M}}{T} - \frac{V_1(T)}{2T}$.

Hence, one can conclude that in the normal situation with real μ and L_f the singularity in $P(\mu,T)$ is absent; this conclusion implies that there is no critical point $T_c(\mu)$ in the domain of small baryon chemical potentials and the analytic structure is affected only by complex singularities. From this point of view, it seems that our consideration could be extended without any changes to large enough values of the chemical potential and temperatures $T \leq 1$ GeV if we take $\bar{M}$ and L independent of μ.

To test ourselves, we have calculated the pressure at $\mu_B = 100$, 200, 300 MeV and $\mu_B = 400$ MeV. As will be seen in the next section, there is reasonable agreement between our predictions and lattice data, without significant changes in the QGP state with growing μ_B.

V. RESULTS AND DISCUSSION

Below, we show our results for the pressure and the sound velocity in comparison with the lattice data. As was discussed above, we obtained the Polyakov line expression via connection with the heavy-light meson mass, derived from the quark condensate using Eq. (17). The exploited form of the Polyakov line $L_{\rm FCM}$ is shown in Fig. 1 together with the dark region $L_{\rm HL}(T)$ derived from the quark condensate. One can see that $L_{\rm FCM}$ is close to the $L_{\rm HL}$ within its accuracy region.

The data for $M_f(T)$ and $M_{\rm adj}(T) = \frac{3}{2}M_f(T)$ are taken from the exponential approximation of the square root expression in Eqs. (9) and (12), which was taken as $M_f(T) = 1.6\sqrt{\sigma^H}$, which is near the Debye mass value, obtained in Ref. [66], and ensures the high-temperature behavior of $P(T)$, which is impossible to reproduce without this CMC contribution.

One can see in Fig. 2 the comparison of our FCM result for $P(T)$ with the lattice data [47,50] for the zero baryon density. The resulting curves coincide within their accuracy limits.

Even more appealing is the agreement of our FCM results for the pressure for $\mu_B = 0.1 \cdot 0.2 \cdot 0.3$ GeV in Fig. 5, respectively, with the lattice data of Ref. [32] for the same values of μ_B. One can conclude that at low μ_B, $\mu_B \leq 0.4$ GeV the FCM results predict a smooth behavior of $P(T,\mu_B)$ without any hint of a singular point, and this is in agreement with the analytic structure of $P(T,\mu_B)$ displayed in Eqs. (22) and (23). At the same time, these results agree with the similar conclusions of the lattice studies [32]. The slight disagreement with the lattice data $\mu_B = 400$ MeV (black solid line) in Fig. 6 could be connected with renormalization of the Polyakov line at finite baryon densities; for example, in Fig. 6, we also show the pressure (gray solid line) with the Polyakov line, that is scaled similarly as in Ref. [74]. One should notice that the

[3]We extended our results to rather high temperatures, just because we wanted to test our basic principles. The same is true for the speed of sound in gluodynamics [72].

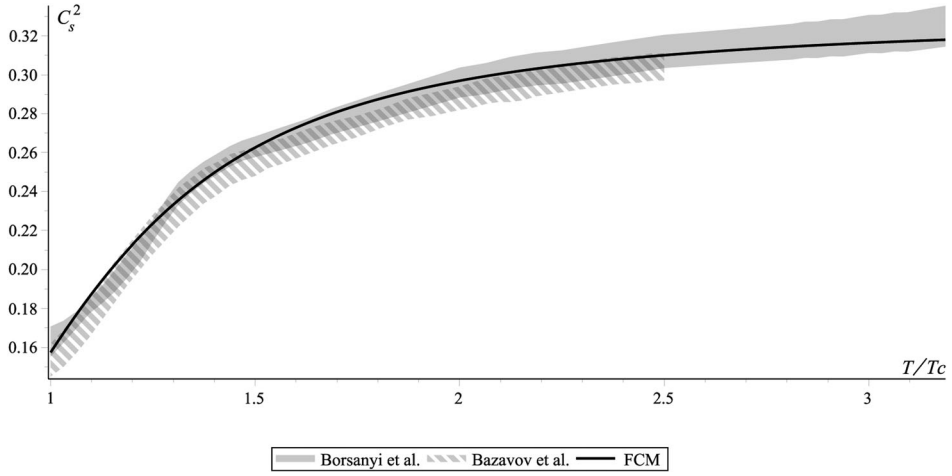

FIG. 4. The square of the speed of sound in QGP as a function of T/T_c. The gray band is the lattice data of Borsanyi *et al.* [20], and the striped band is the lattice data from Bazavov *et al.* [23].

lattice results for the pressure in Ref. [32] were obtained in the first order of the square of the chemical potential.

The square of the speed of sound, which for nonzero μ and in the isentropic condition can be written as (see Appendix D for details of derivation)

$$c_s^2 = \frac{n^2 \frac{\partial^2 P}{\partial T^2} - 2sn \frac{\partial^2 P}{\partial T \partial \mu} + s^2 \frac{\partial^2 P}{\partial \mu^2}}{(\varepsilon + p)\left(\frac{\partial^2 P}{\partial T^2}\frac{\partial^2 P}{\partial \mu^2} - \left(\frac{\partial^2 P}{\partial T \partial \mu}\right)^2\right)}, \tag{24}$$

where we have defined

$$s = \frac{\partial P}{\partial T}, \qquad n = \frac{\partial P}{\partial \mu}, \qquad \varepsilon + P = Ts + \mu n. \tag{25}$$

We show in Fig. 7 the speed of sound in the range $\mu_B = [0, 300]$ MeV, where the width of the line is equal to the difference $c_s^2(\mu_B = 300) - c_s^2(\mu_B = 0)$. So, from the FCM point of view, the domain of low chemical potentials $\mu_B < 400$ MeV is safe and could be described by Taylor

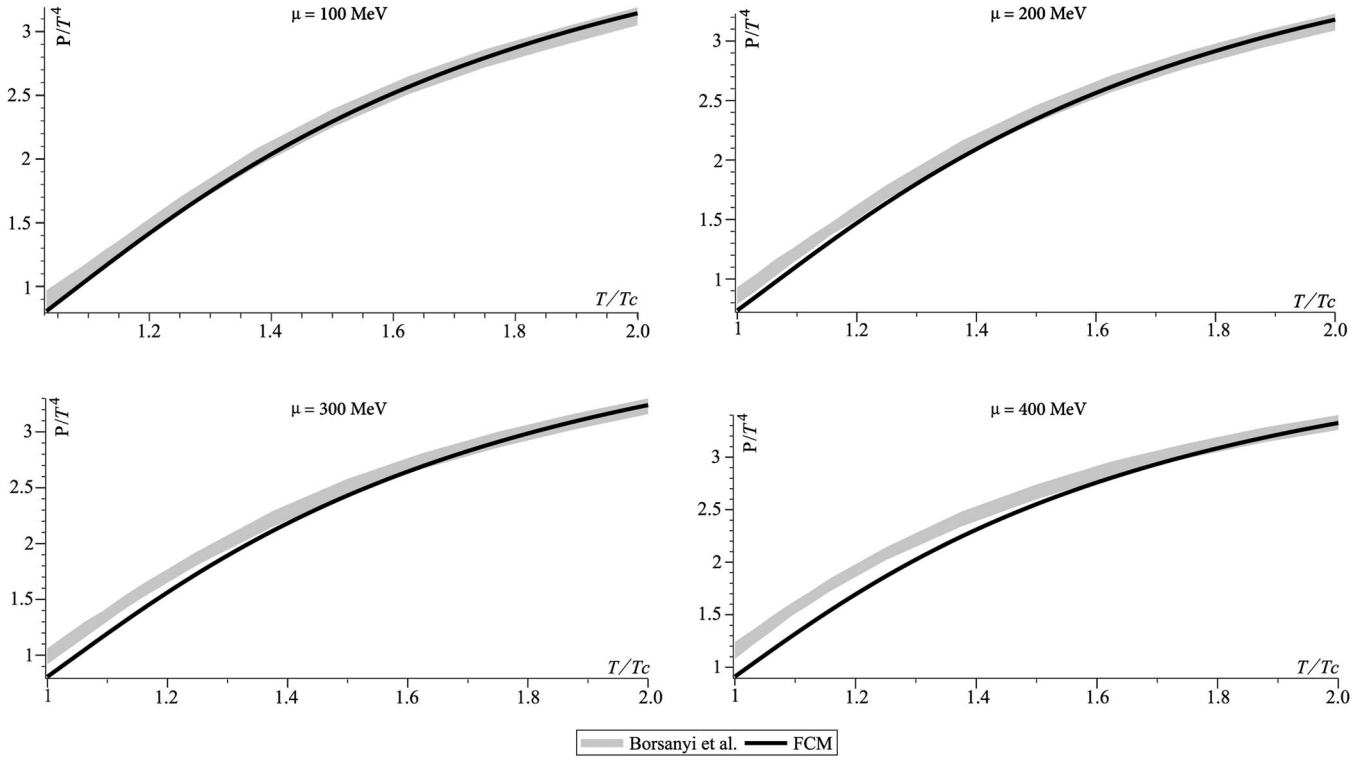

FIG. 5. The ratio of QGP pressure to T^4 as a function of T/T_c for $\mu_B = 100, 200, 300, 400$ MeV. The gray bands are the lattice data of Borsanyi *et al.* from Ref. [32] at corresponding values of μ_B.

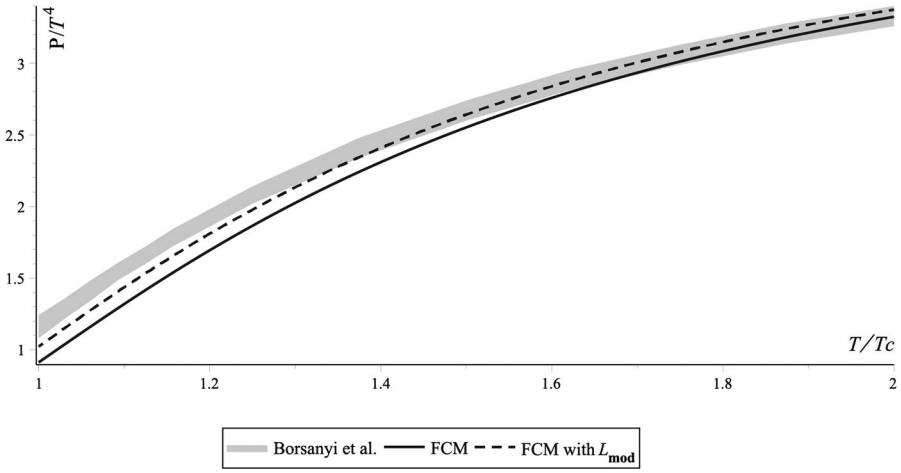

FIG. 6. The ratio of QGP pressure to T^4 as a function of T/T_c for $\mu_B = 400$ MeV with $L_{\rm FCM}$ (black line) and with the Polyakov line that is scaled similarly as in Ref. [74] (dashed line). The gray band is the lattice data of Borsanyi *et al.* from Ref. [32].

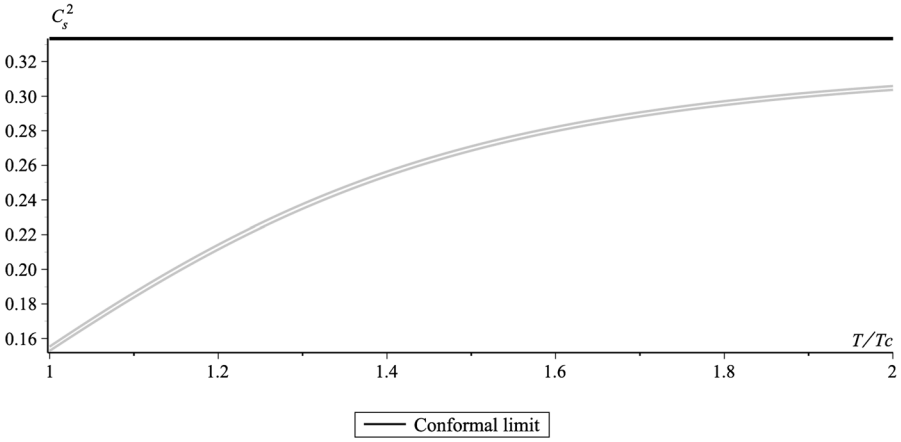

FIG. 7. The width of solid line is the changing of the square of the speed of sound in the range $\mu_B = 0$–300 MeV.

expansion in baryon chemical potential μ_B because in this range this series converges, and the radius of convergences is defined by the $\frac{\mu}{T} = \pm i\pi$ Roberge-Weiss point in Eq. (23).

VI. CONCLUSIONS

The present paper is devoted to the effects of small baryon chemical potential $\mu_B \leq 400$ MeV in the dynamics of QGP.

It is an extension of the study of QCD thermodynamics at vanishing baryon density and is in the line of the series of papers [44–52] in which the QCD thermodynamics is worked out on the basis of the FCM.

We have exploited above the FCM thermodynamics to calculate the QGP pressure at finite baryon density in the temperature range $1 < T/T_c < 2$, where $T_c = 160$ MeV.

Our basic dynamics was defined by two factors: the Polyakov line that is connected with $L_{\rm HL}(T) = \exp(-M_{\rm HL}/T)$ and the CMC in the exponential form with the CMC quark mass $M_D = c\sqrt{\sigma^H(T)}$, where $c = 1.6$ is close to the $q\bar{q}$ Debye mass in Ref. [66] with $c = 2$.

We have used for the heavy-light mass $M_{\rm HL}(T)$ calculated from the T-dependent string tension $\sigma^E(T)$, defined from the quark condensate $\langle q\bar{q}(T)\rangle$ measured on the lattice. The Polyakov line $L_{\rm FCM}$ exploited in the paper is close to the accuracy limits $L = \exp(-M_{\rm HL}(T)/T)$.

We have demonstrated that the resulting pressure $P_{\rm FCM}(T,\mu)$ is in good agreement with lattice data of the Budapest-Wuppertal [20,32] and Hot QCD groups [23] in both cases for zero and nonzero chemical potentials. We have also calculated changing in the speed of sound that one could compare with Fig. 7 in Ref. [32].

From this point of view, our analytic equations (8) and (22) can be considered as an analytic counterpart of the corresponding lattice data.

All this implies the absence of a critical point in the studied range of T and μ_B from the point of view of the FCM method.

It should be noted, however, that we have used both M_D and $M_{\rm HL}$ independent of μ_B in the range $\mu_B < 400$ MeV.

The interesting region of high μ_B, $\mu_B > 1$ GeV, is possibly hiding a completely different picture, with a singular behavior of pressure and sound velocity, as was found in Ref. [75]. However, this phenomenon is strongly connected with a possible dependence of $L(\mu)$ and $M_D(\mu)$ recently studied on the lattice in Ref. [73]. These results are planned for the next paper.

ACKNOWLEDGMENTS

We thank M. A. Andreichikov and B. O. Kerbikov, M. A. Zubkov, E. A. Fedina, R. A. Abramchuck, and especially S. I. Blinnikov for very fruitful discussions. This work was done in the frame of the scientific project, supported by the Russian Science Foundation Grant No. 16-12-10414.

APPENDIX A: THE FCM FORMALISM IN THERMODYNAMICS

To start the FCM approach in the thermodynamics, one can consider gluons and quarks in the background vacuum fields, which can contain both color-electric and color-magnetic fields. Separating perturbative and vacuum gluonic fields, $A_\mu = B_\mu + a_\mu$, one can calculate the gluon and quark propagators in the lowest order in a_μ and take their vacuum average, as was done in Ref. [76]. In this way, one obtains the free energy and pressure in the lowest order of the standard perturbation theory, but with the full account of the averaged vacuum fields, given by correlators $D(x)$ and $D_1(x)$ in (1). Thus, the free energy of gluons can be written via the gluon propagator in the form [76]

$$\begin{aligned}\frac{1}{T}F_0(B) &= \frac{1}{2}\ln\ \det G(B) - \ln\ \det(-D^2(B)) \\ &= \mathrm{tr}\left\{-\frac{1}{2}\int_0^\infty \zeta(s)\frac{ds}{s}e^{-sG(B)} \right. \\ &\quad \left. + \int_0^\infty \zeta(s)\frac{ds}{s}e^{-sD^2(B)}\right\}, \end{aligned} \tag{A1}$$

where $G(B)$ is the gluon propagator and $D^2(B)$ is the ghost propagator in the background field

$$G^{ab}_{\mu\nu} = -D^2(B)_{ab}\delta_{\mu\nu} - 2gF^c_{\mu\nu}(B)f^{acb}, \tag{A2}$$

$$(D_\lambda)_{ca} = \partial_\lambda\delta_{ca} - gf_{bca}B^b_\lambda, \tag{A3}$$

while $\zeta(s)$ is the standard regularizing factor, $\zeta(s) = \lim \frac{d}{dt}\frac{M^{2t}s^t}{\Gamma(t)}|_{t=0}$, the exact form of which is inessential and is not written in what follows.

Our final results require the vacuum field average of (1) and the introduction of the temperature T. The vacuum averaging is to be done with quadratic combinations of fields B_μ in the exponent in (1), and to this end, one can use the cluster expansion [77]

$$\langle \exp f(B)\rangle_B = \exp\{\langle f(b)\rangle_B + \frac{1}{2}[\langle f^2(B)\rangle_B - \langle f(B)\rangle_B^2] + \cdots\}, \tag{A4}$$

which converges well, as shown in Ref. [41], due to the small vacuum correlation length $\lambda \lesssim 0.2$ fm.

Next is the problem of the gluon (quark) Green's function in the external field, which can be represented as the path integral with the phase factor, containing the external field explicitly—this is called the Fock-Feynman-Schwinger representation [76] and has the following form in the simplest case of the ghost Green's function:

$$(-D^2)_{xy} = \left\langle x\right| \int_0^\infty ds e^{sD^2(B)}|_y\Big\rangle = \int_0^\infty ds (DZ)_{xy} e^{-K}\hat{\Phi}(x,y). \tag{A5}$$

Here,

$$K = \frac{1}{4}\int_0^s d\tau\left(\frac{dz_\mu}{d_\tau}\right)^2, \qquad \hat{\Phi}(x,y) = \exp\ ig\int_y^x B_\mu(z)dz_\mu, \tag{A6}$$

the integral is taken along the trajectory of the ghost $y < z_\mu(\tau) \le x$, and $(Dz)_{xy}$ implies the path integral

$$(Dz)_{xy} = \prod_{m=1}^N \frac{d^4\zeta(m)}{(4\pi\varepsilon)^2}\frac{d^4p}{(2\pi)^4}e^{ip(\sum_m \zeta(m)-x+y))}, \tag{A7}$$

where $\zeta(m)$ is the elementary piece of the path.

In a similar way, the gluon propagator has the same representation (A5) but with an additional factor in (A5) multiplying $\hat{\Phi}(x,y), \hat{\Phi}(x,y) \to \hat{\Phi}(x,y)\times\exp(-2ig\int_0^s d\tau \hat{F}_B(z(\tau))) \equiv \hat{\Phi}_F(x,y)$.

The next step is the introduction of the temperature T within the Matsubara formalism.

In the path integral, the latter implies the only replacement, $(Dz)_{xy} \to (Dz)^w_{xy}$, where the upper index w means the winding path integral, which comes from x to the final point y for the sequence of time intervals, $n\beta \equiv n/T$,

$$\begin{aligned}(Dz)^w_{xy} = \prod_{M=1}^N \frac{d^4\Delta z(m)}{(4\pi\varepsilon)^2} \sum_{n=0,\pm1,\ldots} \\ \times \frac{d^4p}{(2\pi)^4}e^{ip(\sum_m \Delta z(m)-(x-y)-n\beta\delta_{\mu 4})}. \end{aligned} \tag{A8}$$

As is seen in (A8), the term with $n = 0$ would yield the T-independent contribution to the pressure, contradicting the free gluon gas result, and should be omitted in what follows. The sum over $n = \pm1, \pm2$ gives the twice of the sum over $n = 1, 2, 3, \ldots$. As it is, only closed trajectories with $x = y$ are entering in the free energy (pressure).

As a result, the pressure $P_{gl}V_3 = -\langle F_0(B)\rangle$ can be written as follows:

$$P_{gl} = T\int_0^\infty \frac{ds}{s}\frac{d^4x}{V_3}(Dz)^w_{xx}e^{-K}\left[\frac{1}{2}\mathrm{tr}\langle\tilde{\Phi}_F(x,x)\rangle - \langle \mathrm{tr}\tilde{\Phi}(x,x)\rangle\right]. \tag{A9}$$

As is clear in (A9), the difference in the square brackets contains two effects: 1) the ghost reduction of the gluon degree of freedom and 2) the gluon spin interaction corrections, since the operator $\hat{F}_{\mu\nu}$ entering in $\hat{\Phi}_F$ has the representation

$$-2i\hat{F}_{\mu\nu} = 2(\mathrm{SB}^{(1)} + \mathrm{S}^{(1)}\varepsilon^{(1)})_{\mu\nu}, \tag{A10}$$

where $\mathbf{S}^{(1)}$ is the gluon spin operator and $\mathbf{B}^{(1)}$ and $\varepsilon^{(1)}$ are the background color-magnetic and color-electric fields.

Therefore, neglecting at the first step the spin-dependent contribution, one can replace the term in the square brackets simply by the adjoint Wilson loop, and as a result, one obtains the representation, given below in (1). It is easy to understand the form (1), considering the free case with vacuum fields $B_\mu \equiv 0$. In this case, as demonstrated in the Appendix of Ref. [76], one obtains from the square brackets in (A9) $(\frac{1}{2}\cdot 4 - 1)(N_c^2 - 1) = N_c^2 - 1$ and

$$P_{gl}(B=0) = \varphi(B=0) = (N_c^2-1)\frac{T^4\pi^2}{45}. \tag{A11}$$

Summarizing, the final result for the gluon pressure can be written in the form Eq. (3) [44,47,49].

APPENDIX B: COLOR-MAGNETIC CONFINEMENT CONTRIBUTION TO $S_3(s)$ AND $G_3(s)$

As one can see in (8), $G_3(s)$ $[S_3(s)]$ contains the contribution of the adjoint (fundamental) loops, which are subject to the area law, $\langle \hat{\mathrm{tr}}_i W_3\rangle = \exp(-\sigma_i\, \mathrm{are} a(W))$ $i = $ fund, adj. The kinetic term is in K_{3d} in (8), so both $G_3(s)$ and $S_3(s)$ are proportional to the Green's functions of two color charges, connected by a confining string, from one point x on the loop to another (arbitrary) point, e.g., the point u on the same loop. As is shown in Ref. [51], one can represent $G_3(s)$ in the spectral sum form,

$$G_3(s) = \frac{1}{\sqrt{\pi s}}\sum_{\nu=0,1,2,..}\psi_\nu^2(0)e^{-2m_\nu^2 s}, \tag{B1}$$

where m_ν are eigenvalues of the Hamiltonian of two adjoint charges, connected by the string, and $\psi_\nu(x)$ is its eigenfunction in two dimensions.

As was discussed in Ref. [51], the spectral sum in (B1) does not converge well, especially at large T, therefore one should calculate the combined effect of all terms. A simple example is given by the free case: $\sigma_i = 0$. In this case, one has

$$G_3^{(0)}(s) = S_3^{(0)}(s) = \frac{1}{\sqrt{\pi s}}\int\frac{d^2p}{(2\pi)^2}e^{-2p^2 s} = \frac{1}{(4\pi s)^{3/2}}. \tag{B2}$$

In this case, one obtains the results for P_{gl} and P_q, which have been found before in Ref. [46],

$$P_{gl}^{(1)} = \frac{2(N_c^2-1)T^3}{\pi^2}\sum_{n=1,2,..}\frac{L_{adj}^{(n)}}{n^4},$$
$$P_q^{(1)} = \frac{4N_cT^4}{\pi^2}\sum_{n=1,2,..}(-1)^{n+1}L_f^{(n)}\varphi_q^{(n)}, \tag{B3}$$

where $\varphi_q^{(n)}$ is

$$\varphi_q^{(n)} = \frac{n^2m_q^2}{2T^2}K_2\left(\frac{nm_q}{T}\right). \tag{B4}$$

One can see in (B3) the Stefan-Boltzmann limit—for $L_{\mathrm{adj}} = L_f = 1$.

There are two ways the CM confinement can be taken into account, suggested in Ref. [51]. Considering the oscillator interaction between the charges, one obtains

$$G_3^{\mathrm{OSC}}(s) = \frac{1}{(4\pi)^{3/2}\sqrt{s}}\frac{M_{\mathrm{adj}}^2}{sh M_{\mathrm{adj}}^2 s}, \tag{B5}$$

and $S_3^{\mathrm{OSC}}(s)$ is obtained from (B5), replacing M_{adj} by M_f. Here, $M_{\mathrm{adj}} = 2\sqrt{\sigma_s} = m_D(T)$, where $m_D(T)$ is the Debye mass, calculated in Ref. [66] in good agreement with lattice data.

A more realistic form is obtained when one replaces the linear interaction $\sigma_s r \to \frac{\sigma_s}{2}(\frac{r^2}{\gamma} + \gamma)$, varying the parameter γ in the final expressions, imitating in this way linear interaction by an oscillator potential. Following Ref. [49], one obtains

$$G_3^{\mathrm{lin}}(s) = \frac{1}{(4\pi s)^{3/2}}\left(\frac{M_{\mathrm{adj}}^2 s}{sh(M_{\mathrm{adj}}^2 s)}\right)^{1/2},$$
$$S_3^{\mathrm{lin}}(s) = G_3^{\mathrm{lin}}(s)|_{M_{\mathrm{adj}}\to M_f}. \tag{B6}$$

Finally, substituting these expressions in (8) and (11), one obtains the equations for P_{gl}^{lin} and P_q^{lin}, containing the effects of CM confinement, which will be used in what follows. However, to simplify the square-root expressions, one can use for $M^2 s \lesssim 1$ the approximation with the square root term replaced by the exponential, $(\frac{M^2 s}{sh M^2 s})^{1/2} \approx \exp(-\frac{M^2 s}{4})$, which has a reasonable accuracy for $T < 1$ GeV.

APPENDIX C: NONPERTURBATIVE CONTRIBUTION TO THE POLYAKOV LINE

The contribution of $D_1^E(x)$ and $D^E(x)$ to the $q\bar{q}(gg)$ interaction can be written in terms of local potentials $V_D(r)$, $V_D^{\rm sat}(r)$, $V_1^E(r)$, $V_c(r)$, and $V_s s(r)$, which will be neglected below. Here, $V_D(r)=\sigma r$, $V_c(r)=-\frac{4\alpha_s}{3r}$, and

$$V_D^{\rm conf}(r,T)=2r\int_0^{1/T}d\nu(1-\nu T)\int_0^r d\xi D^E\left(\sqrt{\xi^2+\nu^2}\right) \tag{C1}$$

$$V_D^{\rm sat}(r,T)=2\int_0^{1/T}d\nu(1-\nu T)\int_0^r \xi d\xi D^E\left(\sqrt{\xi^2+\nu^2}\right) \tag{C2}$$

$$V_1^{\rm sat}(r,T)=\int_0^{1/T}d\nu(1-\nu T)\times\int_0^r \xi d\xi D_1^E\left(\sqrt{\xi^2+\nu^2}\right)-V_1^{\rm Coul}(r,T). \tag{C3}$$

The contributions of V_1^E and $V_D^{\rm sat}$ are strongly compensated as shown in Ref. [70], so one is left with $V_D(r)$ and $V_c(r)$; the latter is effective mostly at large T, when L is close to unity. Therefore, one should take into account the potential $V_D(r)=\sigma r$, which gives rise to the heavy-light bound state with the mass $M_{\rm HL}$ and $L=\exp(-\frac{M_{\rm HL}}{T})$. At this point, it is important to fix the renormalization procedure of the contributing confinement and Coulomb interaction, which is similar in the lattice data of Ref. [78] and in our case and yields almost similar results for $L(T)$, as is seen in Ref. [70].

APPENDIX D: DERIVATION OF EQ. (24) FOR THE SOUND VELOCITY AT FINITE μ

Below, we are interested in the sound velocity c_s at fixed isentropy s/n_B, $c_s^2=(\frac{\partial P}{\partial\epsilon})_{s/n_B}$; $\frac{s}{n_B}\equiv\bar{s}$,

$$\left.\frac{\partial P}{\partial\epsilon}\right|_{\bar{s}}=\frac{\frac{\partial P}{\partial T}dT+\frac{\partial P}{\partial\mu}d\mu}{\frac{\partial\epsilon}{\partial T}dT+\frac{\partial\epsilon}{\partial\mu}d\mu},\qquad \bar{s}=\frac{\frac{\partial P}{\partial T}/\mu}{N}=\text{const.} \tag{D1}$$

Taking into account the isentropic condition

$$d\left(\frac{s}{n_B}\right)=0=d\left(\frac{\frac{\partial P}{\partial T}}{\frac{\partial P}{\partial\mu}}\right)=\frac{d\left(\frac{\partial P}{\partial T}\right)\frac{\partial P}{\partial\mu}-\frac{\partial P}{\partial T}d\frac{\partial P}{\partial\mu}}{\left(\frac{\partial P}{\partial\mu}\right)^2}=\frac{\frac{\partial P}{\partial\mu}\left(\frac{\partial^2 P}{\partial T^2}dT+\frac{\partial^2 P}{\partial T\partial\mu}d\mu\right)-\frac{\partial P}{\partial T}\left(\frac{\partial^2 P}{\partial\mu\partial T}dT+\frac{\partial^2 P}{\partial\mu^2}d\mu\right)}{\left(\frac{\partial P}{\partial\mu}\right)^2}=0, \tag{D2}$$

one obtains the relative change of T and $\mu\div\frac{dT}{d\mu}$,

$$\frac{dT}{d\mu}=\frac{\frac{\partial^2 P}{\partial\mu^2}\frac{\partial P}{\partial T}-\frac{\partial^2 P}{\partial\mu\partial T}\frac{\partial P}{\partial\mu}}{\frac{\partial^2 P}{\partial T^2}\frac{\partial P}{\partial\mu}-\frac{\partial^2 P}{\partial\mu\partial T}\frac{\partial P}{T}}=\frac{a}{b}. \tag{D3}$$

As a result, one obtains from (D1) (dividing the numerator and denominator by $D\mu$)

$$c_s^2=\frac{\frac{\partial P}{\partial T}a+\frac{\partial P}{\partial\mu}b}{\frac{\partial\epsilon}{\partial T}a+\frac{\partial\epsilon}{\partial\mu}b}, \tag{D4}$$

where a and b are given in (D3).

Now, taking into account that $s=\frac{\partial P}{\partial T}$, $n=\frac{\partial P}{\partial\mu}$, $\epsilon+P=Ts+\mu n$, one obtains the final form, given in the text:

$$c_s^2=\frac{n^2\frac{\partial^2 P}{\partial T}-2sn\frac{\partial^2 P}{\partial T\partial\mu}+s^2\frac{\partial^2 p}{\partial\mu^2}}{(\varepsilon+P)\left(\frac{\partial^2 P}{\partial T^2}\frac{\partial^2 P}{\partial\mu^2}-\left(\frac{\partial^2 P}{\partial T\partial\mu}\right)^2\right)}. \tag{D5}$$

[1] J. Adams *et al.* (STAR Collaboration), Nucl. Phys. **A757**, 102 (2005).
[2] K. Adcox *et al.* (PHENIX Collaboration), Nucl. Phys. **A757**, 184 (2005).
[3] I. Arsene *et al.* (BRAHMS Collaboration), Nucl. Phys. **A757**, 1 (2005).
[4] M. Gyulassy and L. McLerran, Nucl. Phys. **A750**, 30 (2005).
[5] B. B. Back *et al.* (PHOBOS Collaboration), Nucl. Phys. **A757**, 28 (2005).
[6] E. V Shuryak, Rev. Mod. Phys. **89**, 035001 (2017); Prog. Part. Nucl. Phys. **62**, 48 (2009).
[7] P. Braun-Munzinger, V. Koch, T. Schafer, and J. Stachel, Phys. Rep. **621**, 76 (2016).
[8] W. Busza, K. Rajagopal, and W. van der Schee, Annu. Rev. Nucl. Part. Sci. **68**, 339 (2018).
[9] R. Pasechnik and M. Šumbera, Universe **3**, 7 (2017).
[10] R. D. Pisarski and F. Wilczek, Phys. Rev. D **29**, 33841 (1984).
[11] G. F. Chapline, M. H. Johnson, E. Teller, and M. S. Weiss, Phys. Rev. D **8**, 4302 (1973).
[12] J. C. Collins and M. J. Perry, Phys. Rev. Lett. **34**, 1353 (1975).
[13] T. D. Lee, Phys. Rev. D **19**, 1802 (1979).

[14] N. Cabibbo and G. Parisi, Phys. Lett. **59B**, 67 (1975).
[15] E. V. Shuryak, Zh. Eksp. Teor. Fiz. **74**, 408 (1978) [Sov. Phys. JETP **47**, 212 (1978)].
[16] R. Snellings, New J. Phys. **13**, 055008 (2011).
[17] D. A. Teaney, arXiv:0905.2433.
[18] T. Hirano and M. Gyulassy, Phys. A **769**, 71 (2006).
[19] S. Borsanyi, Z. Fodor, C. Hoelbling, S. D. Katz, S. Krieg, C. Ratti, and K. K. Szabó, J. High Energy Phys. 09 (2010) 073.
[20] S. Borsanyi, Z. Fodor, and C. Hoelbling, Phys. Lett. B **730**, 99 (2014).
[21] F. Karsch, J. Phys. Conf. Ser. **46**, 122 (2006); J. Goswanu *et al.*, *Proc. Sci.*, LATTICE2018 (2018) 162.
[22] O. Philipsen, Prog. Part. Nucl. Phys. **70**, 55 (2013).
[23] A. Bazavov, T. Bhattacharya, C. DeTar *et al.*, Phys. Rev. D **90**, 094503 (2014).
[24] S. Borsanyi, G. Endrodi, Z. Fodor, A. Jakovác, S. D. Katz, S. Krieg, C. Ratti, and K. K. Szabó, J. High Energy Phys. 11 (2010) 077.
[25] Y. Aoki, G. Endrődi, Z. Fodor, S. D. Katz, and K. K. Szabó, Nature (London) **443**, 675 (2006).
[26] P. Parotto, M. Bluhm, D. Mroczek *et al.*, arXiv:1805.05249.
[27] T. Fischer, N.-U. F. Bastian, M.-R. Wu, P. Baklanov, E. Sorokina, S. Blinnikov, S. Typel, T. Klähn, and D. B. Blaschke, https://www.nature.com/articles/s41550-018-0583-0.
[28] LIGO Scientific and Virgo Collaborations, Phys. Rev. Lett. **119**, 161101 (2017).
[29] N. Itoh, Prog. Theor. Phys. **44**, 291 (1970).
[30] E. Witten, Phys. Rev. D **30**, 272 (1984).
[31] A. Bazavov, H.-T. Ding, P. Hegde *et al.*, Phys. Rev. D **95**, 054504 (2017).
[32] S. Borsanyi, G. Endrodi, Z. Fodor, S. D. Katz, S. Krieg, C. Ratti, and K. K. Szabo, J. High Energy Phys. 08 (2012) 053.
[33] J. Gunther, R. Bellwied, S. Borsanyi, Z. Fodor, S. D. Katz, A. Pasztor, and C. Ratti, Nucl. Phys. **A967**, 720 (2017).
[34] V. G. Bornyakov, V. Braguta, E. M. Ilgenfritz, A. Y. Kotov, A. V. Molochkov, and A. A. Nikolaev, J. High Energy Phys. 03 (2018) 161.
[35] V. V. Braguta, E.-M. Ilgenfritz, A. Y. Kotov, A. V. Molochkov, and A. A. Nikolaev, Phys. Rev. D **94**, 114510 (2016).
[36] V. V. Braguta, E.-M. Ilgenfritz, A. Y. Kotov, B. Petersson, and S. A. Skinderev, Phys. Rev. D **93**, 034509 (2016).
[37] V. V. Braguta, E.-M. Ilgenfritz, A. Y. Kotov, A. V. Molochkov, M. Müller-Preussker, and B. Petersson, J. High Energy Phys. 06 (2015) 094.
[38] H. G. Dosch, Phys. Lett. B **190**, 177 (1987).
[39] H. G. Dosch and Y. A. Simonov, Phys. Lett. B **205**, 339 (1988).
[40] Y. A. Simonov, Nucl. Phys. **B307**, 512 (1988).
[41] A. Di Giacomo, H. G. Dosch, V. I. Shevchenko, and Y. A. Simonov, Phys. Rep. **372**, 319 (2002).
[42] Y. A. Simonov, Phys. Usp. **39**, 313 (1996).
[43] D. S. Kuzmenko, V. I. Shevchenko, and Y. A. Simonov, Phys. Usp. **174**, 3 (2004).
[44] Y. A. Simonov, Ann. Phys. (Amsterdam) **323**, 783 (2008).
[45] E. V. Komarov and Y. A. Simonov, Ann. Phys. (Amsterdam) **323**, 1230 (2008).
[46] Y. A. Simonov and M. A. Trusov, Phys. Lett. B **650**, 36 (2007).
[47] A. V. Nefediev, Y. A. Simonov, and M. A. Trusov, Int. J. Mod. Phys. E **18**, 549 (2009).
[48] N. O. Agasian, M. S. Lukashov, and Y. A. Simonov, Mod. Phys. Lett. A **31**, 1650222 (2016).
[49] N. O. Agasian, M. S. Lukashov, and Y. A. Simonov, Eur. Phys. J. A **53**, 138 (2017).
[50] M. S. Lukashov and Y. A. Simonov, Pis'ma Zh. Eksp. Teor. Fiz. **105**, 659 (2017) [JETP Lett. **105**, 691 (2017)].
[51] M. A. Andreichikov, M. S. Lukashov, and Y. A. Simonov, Int. J. Mod. Phys. A **33**, 1850043 (2018).
[52] M. A. Andreichikov and Y. A. Simonov, Eur. Phys. J. C **78**, 5 (2018).
[53] O. Kaczmarek, F. Karsch, E. Laermann, and M. Lütgemeier, Phys. Rev. D **62**, 034021 (2000).
[54] P. Bicudo and N. Caroso, Phys. Rev. D **85**, 077501 (2012).
[55] P. Cea, L. Cosmai, F. Cuteri, and A. Papa, J. High Energy Phys. 06 (2016) 033.
[56] A. Bazavov, Y. Burnier, and P. Petreczky, Nucl. Phys. **A932**, 117 (2014).
[57] S. Borsanyi, C. Hoelbling, Z. Fodor *et al.*, *Proc. Sci.*, Lattice2010 (2014) 185.
[58] Y. A. Simonov, Phys. Atom. Nucl. D **60**, 2069 (1997).
[59] Y. A. Simonov, Phys. At. Nucl. **67**, 846 (2004).
[60] Y. A. Simonov, Phys. At. Nucl. **67**, 1027 (2004).
[61] Y. A. Simonov, Phys. Rev. D **99**, 056012 (2019).
[62] B. S. De Witt, Phys. Rev. **162**, 1195 (1967); G.'t Hooft, Nucl. Phys. **B62**, 444 (1973).
[63] Y. A. Simonov, Phys. At. Nucl. **74**, 1223 (2011).
[64] Y. A. Simonov, Phys. Rev. D **96**, 096002 (2017).
[65] Y. A. Simonov, Phys. Lett. B **619**, 293 (2005).
[66] N. O. Agasian and Y. A. Simonov, Phys. Lett. B **639**, 82 (2006).
[67] M. D'Elia, A. Di Giacomo, and E. Meggiolaro, Phys. Rev. D **67**, 114504 (2003).
[68] G. Boyd, J. Engels, F. Karsch, E. Laermann, C. Legeland, M. Lütgemeier, and B. Petersson, Nucl. Phys. **B469**, 419 (1996); G. S. Bali, J. Fingberg, U. M. Heller, F. Karsch, and K. Schilling, Phys. Rev. Lett. **71**, 3059 (1993); F. Karsch, E. Laermann, and M. Lütgemeier, Phys. Lett. B **346**, 94 (1995).
[69] A. V. Nefediev and Y. A. Simonov, Phys. At. Nucl. **71**, 171 (2008).
[70] R. A. Abramchuk, Z. V. Khaidukov, and Y. A. Simonov, arXiv:1812.01998.
[71] Y. S. Kalashnikova, A. V. Nefediev, and Y. A. Simonov, Phys. Rev. D **64**, 014037 (2001).
[72] Z. V. Khaidukov, M. S. Lukashov, and Y. A. Simonov, Phys. Rev. D **98**, 074031 (2018).
[73] M. D. 'Elia, F. Negro, A. Rucci, and F. Sanfilippo, Phys. Rev. D **100**, 054504 (2019).
[74] M. D'Elia, F. Di Renzo, and M. P. Lombardo, Phys. Rev. D **76**, 114509 (2007).
[75] Z. V. Khaidukov and Y. A. Simonov, arXiv:1811.08970.
[76] Y. A. Simonov, Phys. At. Nucl. **58**, 309 (1995).
[77] N. G. Van Kampen, Phys. Rep. C **24**, 171 (1976).
[78] A. Bazavov, N. Brambilla, H.-T. Ding, P. Petreczky, H.-P. Schadler, A. Vairo, and J. H. Weber, Phys. Rev. D **93**, 114502 (2016).